Annals of the Academy of Romanian Scientists
Edition ONLINE Physics Series
ISSN 2066-8589 Volume **1**, Number **2/2009**

TAKING ENERGY FROM ENVIRONMENT

Eliade ȘTEFĂNESCU[1]

Abstract. *In this paper, we formulate a physical principle, and propose a semiconductor device producing coherent electromagnetic energy by heat absorption from the environment. This device is a superradiant semiconductor chip, included in a Fabry-Perot cavity, and in intimate contact with a huge radiator. This radiator is designed for a very efficient heat transfer from the environment to the semiconductor structure, which by operation becomes colder than the environment. This structure is composed of a packet of n-i-p-n semiconductor elements that we call superradiant transistors, operating by current injection. On the basis of a physical model of the dissipative superradiant dynamics, we recently elaborated in the framework of the quantum theory of open systems, we show that the energy of the electromagnetic field radiated by quantum transitions in the emitter-base junctions is much larger than the energy electrically dissipated by injection of electrons, the energy difference being obtained by heat absorption in the base-collector junction.*

Keywords: superradiant semiconductor chip, heat transfer from the environment, quantum theory of open systems

1. Introduction

The most energy production is based on a discovery made 500'000 years ago: the fire. Nowadays, the most motors or energy generators, called thermal motors/generators, operate by using a burning process (Fig. 1). With an active fluid and an appropriate mechanical system, the heat obtained by burning a fuel is partially converted into usable energy. By the burning process, the temperature of the active fluid is increased from the initial temperature T_0 to the final temperature T_1, while an energy $\nu N\left(T_1-T_0\right)$ is absorbed by this fluid, where N is the number of molecules, and ν is the number of the degrees of freedom. By an adiabatic expansion, while temperature decreases from T_1 to T_2, a usable energy $\nu N\left(T_1-T_2\right)$ is obtained. To close the operation cycle, the temperature of the active fluid is decreased from T_2 to T_0,

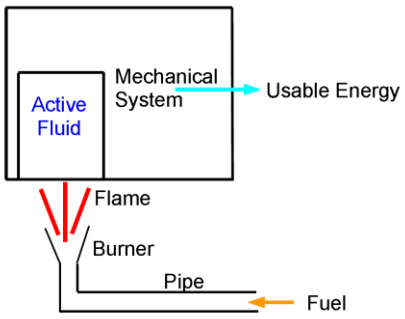

Fig. 1. Motor, converting the heat into usable energy

[1]Center of Advanced Studies in Physics of the Romanian Academy. Founding, full member of the Academy of Romanian Scientists. (e-mail: eliadestefanescu@yahoo.com).

while a residual heat $\nu N(T_2 - T_1)$ is transferred to the environment (Fig. 2). More than that, the operation of a thermal motor burdens the environment not only with the residual heat of the thermal cycle, but also with poisonous chemical residues, resulting from the burning process.

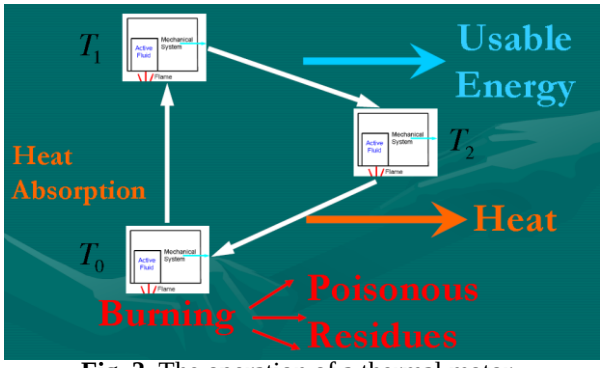

Fig. 2. The operation of a thermal motor.

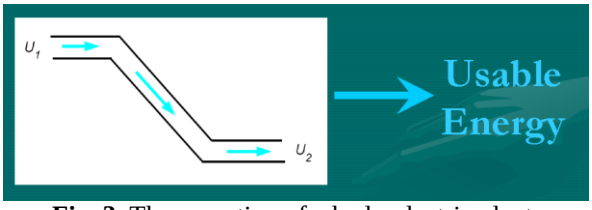

Fig. 3. The operation of a hydroelectric plant.

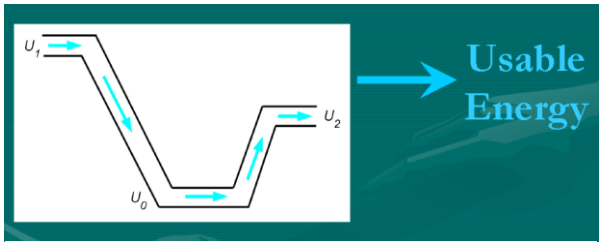

Fig. 4. The operation of a hydroelectric plant with an intermediate lower level.

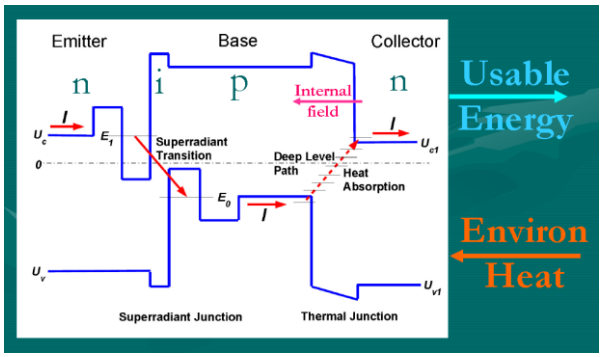

Fig. 5. Superradiant transistor, converting the environmental heat into usable energy.

An ecological method of energy generation is based on the principle of the hydroelectric plant (Fig. 3). In this case, a fall of water from the potential energy U_1 to the potential energy U_2 provides a usable energy $E = U_1 - U_2 - E_L$, where we have taken into account an energy loss E_L. It is interesting to note that in a system with a much lower intermediate state of potential energy $U_0 << U_2 < U_1$, the usable energy remains of the form $E = U_1 - U_2 - E_L$, no matter the large energy fall $U_1 - U_0$ that, in a classical system, is mostly cancelled by the energy raise $U_2 - U_0$ (Fig. 4).

However, in a quantum system, as the semiconductor structure represented in Fig. 5, things are totally different. If the large energy fall $E_1 \to E_0$ is a quantum transition, we can derive advantage from the superradiance effect. In this case, an important part of the energy $E_1 - E_0$ can be extracted outside as a coherent electromagnetic energy flow, which can be easily

converted into electrical energy [1-3]. The electromagnetic power, being an important fraction the decay power $\frac{E_1 - E_0}{e} I$, is much higher than the electric power $(U_c - U_{c1})I$ that is dissipated by the electric current I injected in the device.

We consider a semiconductor device as a packet of superradiant transistors as represented in Fig. 5, in a Fabry-Perot cavity selecting a superradiant mode. In comparison with another device previously proposed by us for converting the environmental heat into electromagnetic energy [4], where the electron transfer through the base-collector junction is made by optical excitations, now we consider a superradiant transistor, with thermal excitation of electrons on a deep-level path. Thus, while a heat is absorbed by the base-collector junctions, a coherent electromagnetic field is generated by the emitter-base junctions due to a superradiance effect. We describe the superradiant quantum transitions by using a quantum master equation we recently derived for a system of fermions in a dissipative environment of other fermions, bosons, and a free electromagnetic field [5].

In this paper, we study the dissipative superradiant dynamics of the system as a function of the main physical parameters of the system for two configurations of the device: (a) a longitudinal device, when the radiation field propagates in the same direction as the injected current, and (b) a transversal device, when the radiation field propagates perpendicularly to the injection current, i.e. in the plane of the semiconductor chip. In Sec. 2, we describe the dynamics of the system as a function of the main couplings involved in the superradiation process: (1) the electric dipole coupling of the active electron system with the superradiant mode, (2) the radiation process of the superradiant field, (3) the dipole-dipole coupling of the active electrons with the quasi-free electrons in the neighboring conduction regions, (4) the polarization fluctuations of the active electrons induced by the thermal fluctuations of the self-consistent field of the conduction electrons, which are a non-Markovian effect, (5) the coupling of the active electrons with the crystal lattice vibrations, (6) the polarization-population coupling induced by multiple reflections in the Fabry-Perot cavity, (7) the coupling of the active electrons with the free electromagnetic field. In Sec. 3, we represent the coefficients of the dissipative superradiant dynamics as functions of the physical parameters of the system. In Sec. 4, we describe the electron excitation with heat absorbsion in the base-collector junction. In Sec. 5, we consider the steady state of the system as a function of the radiation-dissipation characteristics, and study the dependence on the width of the intrinsic zone i of the main parameters of the system: coupling coefficients, dissipation coefficients, the density of quantum dots in the active layer, and the threshold currents. We calculate the radiation

power as a function of the injected current for some values of the device parameters. In Sec. 6, we study the time-dependence of the superradiant power, polarization, and population, when a step current is injected in the device. We show that the thermal fluctuations of the self-consistent field of the conduction electrons induce oscillations of the superradiant power that are not negligible. In Sec. 7 we give some conclusions.

2. Dissipative superradiant dynamics

We describe the dissipative dynamics of a system of electrons interacting with an electromagnetic field by the quantum master equation

$$\frac{d}{dt}\rho(t) = -\frac{i}{\hbar}[H,\rho(t)] - i\sum_{ij}\zeta_{ij}\left[c_i^+c_j,\rho(t)\right] + \sum_{ij}\lambda_{ij}\left(\left[c_i^+c_j\rho(t),c_j^+c_i\right] + \left[c_i^+c_j,\rho(t)c_j^+c_i\right]\right) + \sum_{ijkl}\zeta_{ij}\zeta_{kl}\int_{t-\tau}^{t}\left[c_i^+c_j, e^{-i\left[\phi(t')+\frac{1}{\hbar}H_0^S(t-t')\right]}\left[c_k^+c_l,\rho(t')\right]e^{i\left[\phi(t')+\frac{1}{\hbar}H_0^S(t-t')\right]}\right]dt' \tag{1}$$

with the Hamiltonian

$$H = H_0^S + H^F + V \tag{2}$$

including the terms

$$H_0^S = \sum_k \varepsilon_k c_k^+ c_k \tag{3}$$

for the system of electrons,

$$H^F = \hbar\omega\left(a_+^+a + a_-^+a_- + 1\right) \tag{4}$$

for the two counter-propagating waves of the electromagnetic field in the Fabry-Perot cavity, and

$$V = \frac{e}{M}\vec{p}\vec{A} \tag{5}$$

for the interaction potential. This potential depends on the momentum of the system

$$\vec{p} = iM\sum_{ij}\omega_{ij}\vec{r}_{ij}c_i^+c_j \tag{6}$$

and on the potential vector

$$\vec{A} = \frac{\hbar}{e}\vec{K}\left(a_+e^{ikx} + a_+^+e^{-ikx} + a_-e^{-ikx} + a_-^+e^{ikx}\right) \tag{7}$$

of the electric field

$$\vec{E} = i\frac{\hbar\omega}{e}\vec{K}\left(a_{+}e^{ikx} - a_{+}^{+}e^{-ikx} + a_{-}e^{-ikx} - a_{-}^{+}e^{ikx}\right) \tag{8}$$

propagating in the x-direction. In these expressions, $\hbar\omega_{ij} = \varepsilon_i - \varepsilon_j$ is the energy of a transition $|i\rangle \to |j\rangle$, $\vec{r}_{ij}$ is the dipole moment of this transition, and $\vec{K} = \vec{1}_y\sqrt{\alpha\frac{\lambda}{\mathcal{V}}}$ is a vector in the y-direction of the field, depending on the fine-structure constant $\alpha = \frac{e^2}{4\pi\varepsilon\hbar c} \approx \frac{1}{137}$, the field wavelength $\lambda = \frac{2\pi}{k}$, and the quantization volume of the electromagnetic field $\mathcal{V}$.

The dissipative generator of this equation is composed of a Hamiltonian part with the matrix elements ζ_{ij} that describe transitions stimulated by the fluctuations of the self-consistent field of the environment particles, a Markovian part of Lindblad's form with the decay rates λ_{ij} that describe correlated transitions of the system and environment particles, and a non-Markovian part, as a time-integral of the system operators, describing memory effects, which are proportional to the fluctuations of the self-consistent field of the environment particles. We do not diagonalize the dissipative Hamiltonian $\hbar\sum_{ij}\zeta_{ij}c_i^{+}c_j$ since the matrix elements ζ_{ij} describe fluctuations that arise in any basis of states. The dissipative coefficients of the Markovian part

$$\lambda_{ij} = \lambda_{ij}^{F} + \lambda_{ij}^{B} + \gamma_{ij} \tag{9}$$

include explicit terms for the coupling with an environment of Fermions, Bosons and the free electromagnetic field. These terms depend on the dissipative two-body potentials V^F, V^B, the densities of the environment states $g_\alpha^F(\varepsilon_\alpha)$, $g_\alpha^B(\varepsilon_\alpha)$, the occupation probabilities of these states $f_\alpha^F(\varepsilon_\alpha)$, $f_\alpha^B(\varepsilon_\alpha)$, and temperature T. For a rather low temperature, $T << \varepsilon_{ji}$, $j > i$, these terms are

$$\lambda_{ij}^{F} = \frac{\pi}{\hbar}\left|\langle\alpha i|V^F|\beta j\rangle\right|^2\left[1 - f_\alpha^F(\varepsilon_{ji})\right]g_\alpha^F(\varepsilon_{ji}) \tag{10a}$$

$$\lambda_{ij}^{F} = \frac{\pi}{\hbar}\left|\langle\alpha i|V^F|\beta j\rangle\right|^2 f_\alpha^F(\varepsilon_{ji})g_\alpha^F(\varepsilon_{ji}) \tag{10b}$$

for the Fermi environment of quasi-free electrons,

$$\lambda_{ij}^{B}=\frac{\pi}{\hbar}\left|\langle\alpha i|V^{B}|\beta j\rangle\right|^{2}\left[1+f_{\alpha}^{B}\left(\varepsilon_{ji}\right)\right]g_{\alpha}^{B}\left(\varepsilon_{ji}\right) \tag{11a}$$

$$\lambda_{ij}^{B}=\frac{\pi}{\hbar}\left|\langle\alpha i|V^{B}|\beta j\rangle\right|^{2}f_{\alpha}^{B}\left(\varepsilon_{ji}\right)g_{\alpha}^{B}\left(\varepsilon_{ji}\right) \tag{11b}$$

for the Bose environment of lattice vibrations, and

$$\gamma_{ij}=\frac{2\alpha}{c^{2}\hbar^{3}}\vec{r}_{ij}^{\,2}\varepsilon_{ji}^{3}\left(1+\frac{1}{e^{\varepsilon_{ji}/T}-1}\right) \tag{12}$$

for the Bose environment of the free electromagnetic field, where $\vec{r}_{ij}$ are the transition dipole moments. The terms with the dissipative coefficients (9)-(12) of the master equation (1) describe single-particle transitions of the system and environment, with energy conservation, $\varepsilon_{ji}=\varepsilon_{\alpha\beta}$, in agreement with the quantum-mechanical principles, and with the detailed balance principle [6]. The non-Markovian part of this equation takes into account the fluctuations of the self-consistent field of the environment Fermions, as a function of the coefficients

$$\zeta_{ij}=\frac{1}{\hbar}\sqrt{\frac{1}{Y^{F}}\int_{(\alpha)}\langle\alpha i|\left(V^{F}\right)^{2}|\alpha j\rangle\, f_{\alpha}^{F}\left(\varepsilon_{\alpha}\right)g_{\alpha}^{F}\left(\varepsilon_{\alpha}\right)d\varepsilon_{\alpha}} \tag{13}$$

where Y^{F} is the total number of these particles occupying the states α. In equation (1), $\phi(t')$ is a phase-operator describing fluctuations induced by the thermal fluctuations of the self-consistent field of the environment particles, while τ is a memory time, that is much longer than the fluctuation time of this field, but much shorter than the decay/excitation times and the period of the Rabi oscillation that characterizes the Hamiltonian dynamics. We notice that the fluctuation Hamiltonian $\hbar\sum_{ij}\varsigma_{ij}c_{i}^{+}c_{j}$ in (1) is similar to the hopping Hamiltonian (3) in [7]. Besides this fluctuation Hamiltonian, a non-Markovian term of the second-order in the fluctuation matrix elements ζ_{ij} arises from the dissipative quantum dynamics in the approximation of a weak dissipative coupling.

We consider the quantum master equation (1) for a two-level system and derive optical equations in the approximation of the slowly varying amplitudes of the non-diagonal elements

$$\rho_{10}(t)=\rho_{01}^{*}(t)=\frac{1}{2}\left[S_{+}(t)e^{ikx}+S_{-}(t)e^{-ikx}\right]e^{-i\omega t}, \tag{14}$$

with the amplitude

$$S_{+}(t)=u(t)-iv(t), \tag{15}$$

and of the population difference

$$w(t)=\rho_{11}(t)-\rho_{00}(t), \tag{16a}$$

with the normalization condition

$$1=\rho_{11}(t)+\rho_{00}(t). \tag{16b}$$

At the same time we consider the mean-value electric field is of the form

$$\left\langle \vec{E} \right\rangle = \frac{1}{2}\left[\vec{\mathcal{E}}(t)e^{-i\omega t}+\vec{\mathcal{E}}^{*}e^{i\omega t}\right] \tag{17}$$

with the amplitude

$$\mathcal{E}(t)=\mathcal{E}_{+}(t)e^{ikx}+\mathcal{E}_{-}(t)e^{-ikx} \tag{18}$$

satisfying the boundary condition:

$$\vec{\mathcal{E}}_{-}(t)=-\sqrt{1-\mathcal{T}}\,\vec{\mathcal{E}}_{+}(t), \tag{19}$$

where $\mathcal{T}$ is the transmission coefficient of the output mirror. With a notation similar to (15) for the amplitude of the electric field

$$\mathcal{E}_{+}(t)=\mathcal{F}(t)+i\mathcal{G}(t), \tag{20}$$

from the master equation (1) we get equations of the mean-values:

$$\begin{aligned}\frac{d}{dt}u(t)= & -\gamma_{\perp}\left[u(t)-\delta\omega v(t)\right]-g\mathcal{G}(t)w(t)\\ & +\gamma_n^2\int_{t-\tau}^{t}\left\{u(t')\cos\left[\phi_n(t')+(\omega-\omega_0)(t-t')\right]+v(t')\sin\left[\phi_n(t')+(\omega-\omega_0)(t-t')\right]\right\}dt'\end{aligned} \tag{21a}$$

$$\begin{aligned}\frac{d}{dt}v(t)= & -\gamma_{\perp}\left[v(t)+\delta\omega u(t)\right]-g\mathcal{F}(t)w(t)\\ & +\gamma_n^2\int_{t-\tau}^{t}\left\{v(t')\cos\left[\phi_n(t')+(\omega-\omega_0)(t-t')\right]-u(t')\sin\left[\phi_n(t')+(\omega-\omega_0)(t-t')\right]\right\}dt'\end{aligned} \tag{21b}$$

$$\frac{d}{dt}w(t)=-\gamma_{\parallel}\left[w(t)-w_T\right]+2\mathcal{I}+\left(2-\mathcal{T}\right)g\left[\mathcal{G}(t)u(t)+\mathcal{F}(t)v(t)\right] \tag{21c}$$

$$\frac{d}{dt}\mathcal{F}(t)=-\frac{1}{2}\mathcal{T}c\frac{\mathcal{A}}{\mathcal{V}}\mathcal{F}(t)-\gamma_F\mathcal{F}(t)-g\frac{\hbar\omega_0}{2\varepsilon\mathcal{V}}v(t) \tag{21d}$$

$$\frac{d}{dt}\mathcal{G}(t)=-\frac{1}{2}\mathcal{T}c\frac{\mathcal{A}}{\mathcal{V}}\mathcal{G}(t)-\gamma_F\mathcal{G}(t)-g\frac{\hbar\omega_0}{2\varepsilon\mathcal{V}}u(t) \tag{21e}$$

where $\tau > \tau_n = 1/\gamma_n$,

$$g = \frac{e}{\hbar}\vec{r}_{10}\vec{1}_E \tag{22}$$

is the coupling coefficient of the electron system with the dipole moment $\vec{r}_{10}$ with the electromagnetic field with the polarization vector $\vec{1}_E$,

$$\gamma_\perp = \lambda_{01} + \lambda_{10} \tag{23}$$

is the dephasing rate,

$$\gamma_\parallel = 2(\lambda_{01} + \lambda_{10}) \tag{24}$$

is the decay rate,

$$\gamma_n = |\zeta_{11} - \zeta_{00}| \tag{25}$$

is the fluctuation rate,

$$w_T = -\frac{\lambda_{01} - \lambda_{10}}{\lambda_{01} + \lambda_{10}} \tag{26}$$

is the equilibrium population,

$$\delta\omega = \frac{\omega - \omega_0}{\gamma_\perp} \tag{27}$$

is the relative detuning, $\mathcal{I}$ is the injected electron flow, $\mathcal{V}$ is the quantization volume, $\mathcal{A}$ is the radiation area from the quantization volume, and γ_F is the decay rate of the superradiant field.

3. Dependence on physical parameters

We consider a superradiant device, as a semiconductor chip with the area A_D and the thickness L_D, including a number $\overline{N}_t$ of n-i-p superradiant transistors, in two versions: (a) a longitudinal device with the two mirror metallization M_1 and M_2 made on the two surfaces in the plane of the chip, of transmission coefficients $T_0 = 0$ and $T > 0$, respectively, coupling the superradiant mode that propagates in the x-direction of the injection current (Fig. 6), and (b) a transversal device with the two mirror metallization M_1 and M_2 made on two lateral surfaces of the chip, of transmission coefficients $T_0 = 0$ and $T > 0$, respectively, coupling the superradiant mode that propagates in the y-direction, perpendicular to the injection current (Fig. 7). While in version (a) the roles of mirrors and injection electrodes are played by the metallization $\mathcal{E}_1$ and $\mathcal{E}_2$, made on the two surfaces in the plane of the chip, in version (b) the mirror metallization M_1 and M_2, which are made on two lateral surfaces, are different from the electrode metallization $\mathcal{E}_1$ and $\mathcal{E}_2$.

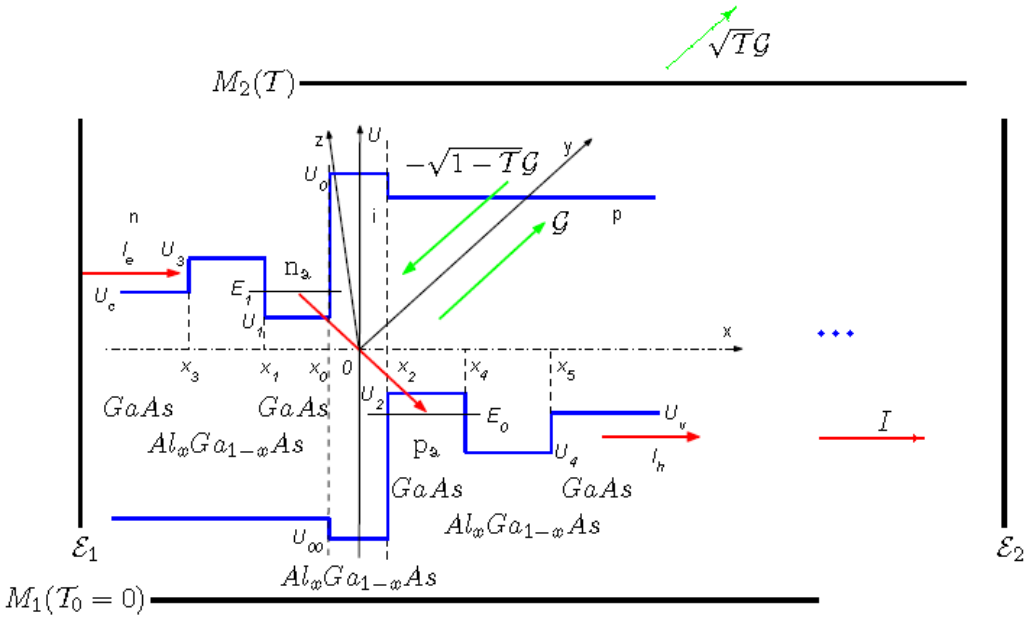

Fig. 6. Superradiant transistor in a longitudinal configuration.

The two devices have the same semiconductor structure including $GaAs$ layers, with a narrower forbidden band and a heavier doping, for the quantum wells, and $Al_xGa_{1-x}As$ layers, with a larger forbidden band and a lighter doping, for the potential barriers.

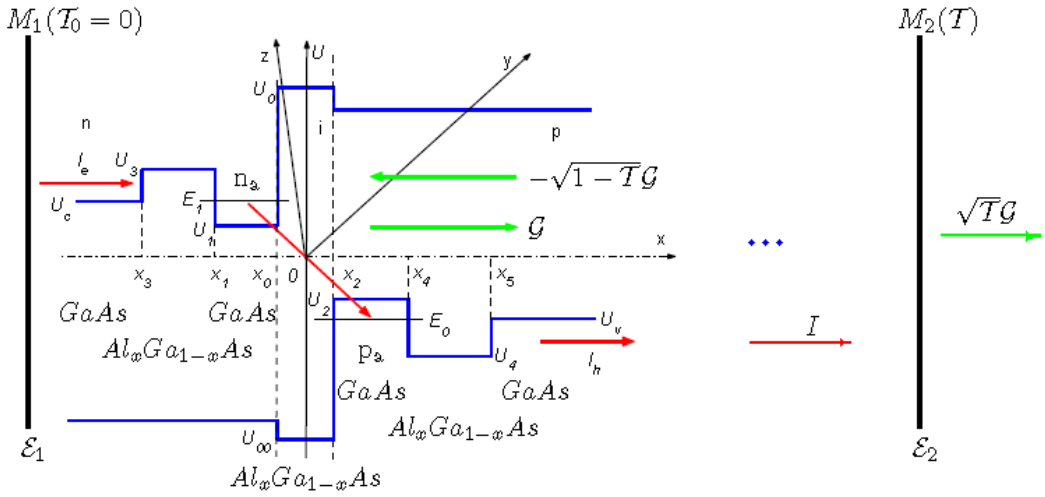

Fig. 7. Superradiant transistor in a transversal configuration.

The margins of these bands are determined by the concentrations of the donors/acceptors embedded in the semiconductor layers. For the potential distribution, we consider a simple rectangular model taking into account the

essential characteristics of the system. The margin $U_c\,(U_v)$ of the conduction (valence) band of the conduction region n (p), depends on the donor (acceptor) concentration $N_D\,(N_A)$, and temperature T:

$$U_c(T)=T\ln\frac{N_c(T)}{N_D},\qquad N_c=2\left(\frac{\sqrt{M_nT/2\pi}}{\hbar}\right)^3 \tag{28a}$$

$$U_v(T)=-T\ln\frac{N_v(T)}{N_A},\qquad N_v=2\left(\frac{\sqrt{M_pT/2\pi}}{\hbar}\right)^3. \tag{28b}$$

The two potentials $U_1,\ U_2$ of the active quantum system depend on the quantum dot density N_e, of pairs of donors and acceptors embedded in the two layers n_a and p_a, respectively, and temperature:

$$U_1(T)=-T\ln\left(e^{\frac{\pi\hbar^2N_e}{M_nT}}-1\right) \tag{29a}$$

$$U_2(T)=T\ln\left(e^{\frac{\pi\hbar^2N_e}{M_pT}}-1\right). \tag{29b}$$

Similar expressions are obtained for the potentials U_3 and U_4 of the separation barriers as functions of the donor and acceptor concentrations N_3 and N_4. The two potential wells U_1 and U_2 have the ground state energies E_1 and E_0 as solutions of the equations:

$$E_1-U_1=\frac{\hbar^2}{2M_n(x_0-x_1)^2}\left(\arctan\sqrt{\frac{U_0-E_1}{E_1-U_1}}+\arctan\sqrt{\frac{U_3-E_1}{E_1-U_1}}\right)^2 \tag{30a}$$

$$U_2-E_0=\frac{\hbar^2}{2M_p(x_4-x_2)^2}\left(\arctan\sqrt{\frac{E_0-U_{00}}{U_2-E_0}}+\arctan\sqrt{\frac{E_0-U_4}{U_2-E_0}}\right)^2. \tag{30b}$$

The superradiant Fabry-Perot cavity of the device, which is resonant to the transition frequency, has a length equal to a an integer number of wave-lengths, with the active zones of the n_a-i-p_a layers placed for the strongest coupling to the superradiant mode, and the p-n quasi-ohmic contacts between two successive junctions placed for the weakest coupling to the superradiant mode. Thus, in a longitudinal device, the active zones are placed at the maximum-field points of

the superradiant cavity, while the quasi-ohmic contacts are placed at the minimum-field points of the cavity. In a transversal device, the active zones are placed at the zero-field points of the cavity formed by the two electrodes $\mathcal{E}_1$ and $\mathcal{E}_2$ of the structure, thus favoring the coupling to the perpendicular superradiant mode. In the longitudinal device, the electromagnetic field is coupled to the dipole moment with the most probable values

$$y_{01}^{(\Psi)} = c_{01}^{(x)} \frac{\hbar}{2\sqrt{M_n T}}, \qquad y_{10}^{(\Psi)} = c_{01}^{(x)} \frac{\hbar}{2\sqrt{M_p T}} \tag{31}$$

due to the quasi-free thermal motion of the electrons at temperature T in the two active arrays of the quantum dot system, where

$$c_{01}^{(x)} = \frac{A_1 A_0}{\alpha_0 - \alpha_1} \sqrt{\frac{(E_1 - U_1)(U_2 - E_0)}{(U_0 - U_1)(U_2 - U_{00})}} \left(e^{-\alpha_1 (x_2 - x_0)} - e^{-\alpha_0 (x_2 - x_0)} \right) \tag{32}$$

is the overlap function of the two states on the x-coordinate, while

$$A_1 = \sqrt{2} \left[x_0 - x_1 + \frac{\hbar}{\sqrt{2M_n}} \left(\frac{1}{\sqrt{U_0 - E_1}} + \frac{1}{\sqrt{U_3 - E_1}} \right) \right]^{-1/2} \tag{33a}$$

$$A_0 = \sqrt{2} \left[x_4 - x_2 + \frac{\hbar}{\sqrt{2M_p}} \left(\frac{1}{\sqrt{E_0 - U_{00}}} + \frac{1}{\sqrt{E_0 - U_4}} \right) \right]^{-1/2} \tag{33b}$$

are normalization coefficients. In the transversal device, the electromagnetic field is coupled to the dipole moment

$$x_{01}^{(\Psi)} = c_{01}^{(x)} \left(\frac{x_2 - x_0}{2} - \frac{1}{\alpha_0 - \alpha_1} \right), \tag{34}$$

determined by the separation distance $x_2 - x_0$ between the two wave-functions of the active system, and their attenuation coefficients α_1, α_0 in the i-zone separating these wave-functions. Both these moments are proportional to the overlap function $c_{01}^{(x)}$ of the x-wave functions in the i-zone. It is interesting that, in the numerical case considered in the next section, these two dipole moments are approximately of the same order of magnitude.

Considering the dipole-dipole coupling of the active electrons with the environment particles, we obtained explicit expressions of the dissipative coefficients. For the decay and dephasing rates (23)-(24), we get

$$\gamma_{\parallel} = 2\gamma_{\perp} = \gamma_{\parallel}^{E} + \gamma_{\parallel}^{P} + \gamma_{\parallel}^{EM}, \tag{35}$$

where $\gamma_{\parallel}^{E}$ stands for the electric coupling to the conduction electrons, $\gamma_{\parallel}^{P}$ for the phonon coupling to the crystal lattice vibrations, and $\gamma_{\parallel}^{EM}$ for the coupling to the free electromagnetic field. The electric decay rate has two components for the interaction with the two conduction regions n and p:

$$\gamma_{\parallel}^{E} = \gamma_{\parallel}^{(n)} + \gamma_{\parallel}^{(p)}. \tag{36}$$

For the two components of the electron decay rates, we get

$$\gamma_{\parallel}^{(n)} = \frac{8\alpha^2 c^2 \sqrt{2M_n}\left(\varepsilon_{10} + \frac{T}{2}\right)\left|c_{01}^{(x)}\right|^2 \mu_{01}^2}{3\left(\frac{N_D^{-1/3}}{2} - x_3\right)^3 \varepsilon_{10}^{3/2}}, \tag{37}$$

and

$$\gamma_{\parallel}^{(p)} = \frac{8\alpha^2 c^2 \sqrt{2M_p}\left(\varepsilon_{10} + \frac{T}{2}\right)\left|c_{01}^{(x)}\right|^2 \mu_{01}^2}{3\left(\frac{N_A^{-1/3}}{2} + x_5\right)^3 \varepsilon_{10}^{3/2}}, \tag{38}$$

where

$$\mu_{01}^2 = \left(\frac{x_2 - x_0}{2} - \frac{1}{\alpha_0 - \alpha_1} + \frac{\hbar}{\sqrt{M_n T}}\right)\left(\frac{x_2 - x_0}{2} - \frac{1}{\alpha_0 - \alpha_1} + \frac{\hbar}{\sqrt{M_p T}}\right). \tag{39}$$

These two expressions describe dipole-dipole couplings of an active electron to the quasi-free electrons in the two conduction regions n and p, which are inverse proportional to the separation distances $\frac{N_D^{-1/3}}{2} - x_3$ and $\frac{N_A^{-1/3}}{2} + x_5$ with power 3, respectively. The electron decay rates (37) and (38) decrease with the transition energy $\varepsilon_{10} = E_1 - E_0$ of an active electron, an increase of this energy leading to transitions of the environment particles into states with wave-functions more rapidly varying in space, and forming smaller dipole moments. The phonon decay rate

$$\gamma_{\parallel}^{P} = \sum_{\alpha} \frac{2E_e^2 \varepsilon_{10}^5 \left(\vec{r}_{01}\vec{1}_{\alpha}\right)\left(\vec{r}_{10}\vec{1}_{\alpha}\right)}{\pi\hbar^6 c^4 v^3 D} \cdot \frac{e^{\varepsilon_{10}/T} + 1}{e^{\varepsilon_{10}/T} - 1} \tag{40}$$

where $E_e = Mc^2$ is the rest energy of the electron and $\vec{1}_{\alpha}$ are the polarization vectors of the phonon modes, essentially depends on the transition energy ε_{10} with power 5, the square of the dipole moments $\vec{r}_{01}$, $\vec{r}_{10}$, temperature T, and the sound velocity

$$v \approx \sqrt{\frac{E}{D}} \tag{41}$$

as a function of the Young elasticity coefficient E and the crystal density D. The electromagnetic decay rate

$$\gamma_{\parallel}^{EM} = \frac{4\alpha\varepsilon_{10}^3 \vec{r}_{01}\vec{r}_{10}}{\hbar^3 c^2} \cdot \frac{e^{\varepsilon_{10}/T}+1}{e^{\varepsilon_{10}/T}-1} \tag{42}$$

also depends on the square of the dipole moment $\vec{r}_{01}$ and temperature T, but on the transition energy ε_{10} with power 3. In the numerical case in the next section, the phonon decay rate (40) dominates the electron decay rate (36)-(39), while the electromagnetic decay rate (42) is negligible. The non-Markovian coefficient depends on the relative fluctuations between the two levels, induced by the two components n and p of the environment:

$$\gamma_n^2 = \left(\sqrt{\left[\zeta_{11}^{(n)}\right]^2 + \left[\zeta_{11}^{(p)}\right]^2} - \sqrt{\left[\zeta_{00}^{(n)}\right]^2 + \left[\zeta_{00}^{(p)}\right]^2} \right)^2 \tag{43}$$

where

$$\left(\zeta_{11}^{(n)}\right)^2 = \frac{\alpha^2 c^2 M_n^{3/2} T^{3/2}}{360\pi\sqrt{2\pi}\hbar^3} \cdot \frac{N_D^{1/3}\left[A_1^2\left(x_0^3 - x_1^3\right) + \frac{1}{N_e}\right]}{N_e N_c \left(\frac{N_D^{-1/3}}{2} - x_3 + \frac{x_0 + x_1}{2}\right)^5} \tag{44a}$$

$$\left(\zeta_{11}^{(n)}\right)^2 = \frac{\alpha^2 c^2 M_p^{3/2} T^{3/2}}{360\pi\sqrt{2\pi}\hbar^3} \cdot \frac{N_A^{1/3}\left[A_1^2\left(x_0^3 - x_1^3\right) + \frac{1}{N_e}\right]}{N_e N_v \left(\frac{N_A^{-1/3}}{2} + x_5 - \frac{x_0 + x_1}{2}\right)^5} \tag{44b}$$

$$\left(\zeta_{00}^{(n)}\right)^2 = \frac{\alpha^2 c^2 M_n^{3/2} T^{3/2}}{360\pi\sqrt{2\pi}\hbar^3} \cdot \frac{N_D^{1/3}\left[A_0^2\left(x_4^3 - x_2^3\right) + \frac{1}{N_e}\right]}{N_e N_c \left(\frac{N_D^{-1/3}}{2} - x_3 + \frac{x_4 + x_2}{2}\right)^5} \tag{44c}$$

$$\left(\zeta_{00}^{(p)}\right)^2 = \frac{\alpha^2 c^2 M_p^{3/2} T^{3/2}}{360\pi\sqrt{2\pi}\hbar^3} \cdot \frac{N_A^{1/3}\left[A_0^2\left(x_4^3 - x_2^3\right) + \frac{1}{N_e}\right]}{N_e N_c \left(\frac{N_A^{-1/3}}{2} + x_5 - \frac{x_4 + x_2}{2}\right)^5} \tag{44d}$$

The non-Markovian coefficient (43)-(44) arises due to the distance difference of the two states from the two conduction regions: the field fluctuations of a conduction region have a stronger influence on the closer state than on the farer one. It is interesting to notice that these fluctuations occur like a near-field effect, strongly decreasing with the distance and with the quantum dot density N_e.

4. Electron excitation with heat absorption in the base-collector junction

The superradiant power is a result of the electron transitions with the energy $\hbar\omega_0$ and of the dissipation-radiation processes in the active quantum system as is described by equations (21).

However, the operation of the device is based also on another process, of electron transfer from the p-region of the base to the n-region of the collector. This process involves a quasi-ohmic contact between these two regions, i.e. the existence of a deep-level path crossing the energy gap of the base-collector junction as in Fig. 5. On this deep level path the electrons are carried up by the internal field of the p-n contact junction, while the energy of this field is recovered by heat absorption, by the electrons building up this field by diffusion. This electron transfer by the internal field of a junction is similar to the transistor effect with the difference that in an ordinary bipolar transistor the electrons cross the base-collector junction decaying through the conduction band, with energy dissipation, while here the electrons go up, absorbing energy from the internal field.

This phenomenon can be understood from statistical reasons. From Fig. 5, we notice that the injected current I increases the population of the lower states and decreases the population of the higher states of the deep level path. That means that this region becomes colder, absorbing heat from the environment. This heat absorption has the tendency to remake the initial statistical distribution, modified by current injection.

In the calculations above we neglected the temperature variation due to the heat transfer throughout the semiconductor structure. To take into account this temperature variation, one has to make corrections of the parameters, to obtain the same transition frequency on the whole chain of superradiant junctions.

5. Steady state

From the system of equations (21) for the resonance case ($\delta\omega = 0$), we calculate the flow density of the electromagnetic energy radiated by the device:

$$\mathcal{P} = \mathcal{T}c\frac{1}{2}\varepsilon\left(\mathcal{F}^2 + \mathcal{G}^2\right). \tag{45}$$

We get

$$\mathcal{P} = \frac{\dfrac{\hbar\omega_0}{(2-\mathcal{T})\mathcal{A}}}{1+\dfrac{2\gamma_F \mathcal{V}}{\mathcal{T}c\mathcal{A}}}\left[\mathcal{I} - \left(-w_T\frac{\gamma_\parallel}{2} + \frac{\dfrac{1}{2}\mathcal{T}c\dfrac{\mathcal{A}}{\mathcal{V}} + \gamma_F}{\dfrac{g^2\hbar\omega_0}{\gamma_\perp\gamma_\parallel\varepsilon\mathcal{V}}}\right)\right]. \tag{46}$$

With the radiation areas $\mathcal{A}$ of a quantum dot for a longitudinal and a transversal device, respectively, from (46) we derive the flow densities $\mathcal{P}_L$ and $\mathcal{P}_T$, and the total flows of the electromagnetic field radiated by these devices:

$$\Phi_L = A_D\mathcal{P}_L = \frac{\overline{N}_t}{(2-\mathcal{T})\left(1+2\dfrac{1_L\gamma_F}{\mathcal{T}c}\right)}\cdot\frac{\hbar\omega_0}{e}(I - I_{0L}) \tag{47a}$$

$$\Phi_T = L_D\sqrt{A_D}\mathcal{P}_T = \frac{\overline{N}_t}{(2-\mathcal{T})\left(1+2\dfrac{1_L\gamma_F}{\mathcal{T}c}\cdot\dfrac{A_D^{1/2}}{L_D}\right)}\cdot\frac{\hbar\omega_0}{e}(I - I_{0T}) \tag{47b}$$

as a function of the injected current $I = eN_eA_D\mathcal{I}$ and the threshold currents

$$I_{0L} = \frac{1}{2}eN_eA_D\gamma_\parallel\left[-w_T + \frac{\varepsilon\gamma_\perp}{g_L^2\hbar\omega_0N_e\overline{N}_t}(\mathcal{T}c + 2\cdot 1_L\gamma_F)\right] \tag{48a}$$

$$I_{0T} = \frac{1}{2}eN_eA_D\gamma_\parallel\left[-w_T + \frac{\varepsilon\gamma_\perp}{g_L^2\hbar\omega_0N_e\overline{N}_t}\left(\mathcal{T}c\frac{L_D}{A_D^{1/2}} + 2\cdot 1_L\gamma_F\right)\right], \tag{48b}$$

where we used the notation 1_L for the unit length. The threshold current is proportional to the population threshold that includes three terms for the three dissipative processes that must be balanced by current injection for creating a coherent field: (1) the threshold value $-w_T$, necessary to reach an inversion state of the population, (2) the population inversion proportional to the light velocity c and the transmission coefficient $\mathcal{T}$, necessary to balance the radiation of the field, and (3) the population inversion proportional to decay rate γ_F, necessary to balance the dissipation of the field. The second term arises only due to the openness of the cavity, while for a closed cavity, when $\mathcal{T} = 0$ and no energy is lost by radiation, this term vanishes.

In the following, we study a few essential dependences of the dissipative coefficients. In Fig. 8 we represent the components $\gamma_\parallel^E$, $\gamma_\parallel^P$, $\gamma_\parallel^{EM}$ of the decay rate $\gamma_\parallel$, and the non-Markovian coefficient γ_n as functions of the width $x_2 - x_0$ of

the i-zone that essentially determines the overlap of the two wave functions of the initial and final states and, by this, the transition dipole moment. First of all, we notice that the electromagnetic decay rate $\gamma_{\parallel}^{EM}$ is negligible in comparison with the electric and phonon decay rates $\gamma_{\parallel}^{E}$, $\gamma_{\parallel}^{P}$, and that the phonon decay dominates the other decay processes. We also notice that the variation of the decay rates with the width of the i-zone is very strong, while the dependence of the non-Markovian coefficient γ_n is weak, this coefficient being essentially determined by the distance between the active electrons and the quasi-free electrons in the conduction regions. The non-Markovian coefficient γ_n is much larger than the decay rates, this coefficient describing fluctuations of a mean-time $1/\gamma_n$ much shorter than the decay time $1/\gamma_{\parallel}$.

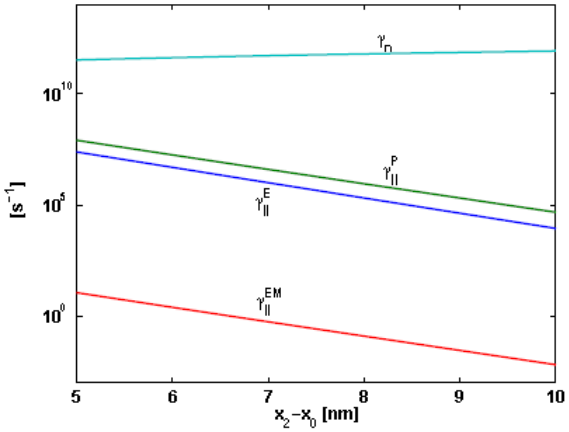

Fig. 8. The dependence of the dissipative coefficients on the width of the i-zone.

In Fig. 9 we represent the dependence on the width $x_2 - x_0$ of the coupling coefficients g_L, g_T. We notice that the two coefficients g_L and g_T are of the same order of magnitude. However, as one can notice also from (31)-(34), the dependence on $x_2 - x_0$ of the coupling coefficient to the transversal mode g_T, which is proportional to $x_{01}^{(\Psi)}$, is weaker than that of the coupling coefficient to the longitudinal mode g_L, which is proportional to $\bar{y}_{01}^{(\Psi)} = \sqrt{y_{01}^{(\Psi)} y_{10}^{(\Psi)}}$.

In Fig. 10 we represent the dependence on the width $x_2 - x_0$ of the threshold currents. The decrease of these currents with $x_2 - x_0$ is determined by the decrease of the decay rate $\gamma_{\parallel}$. The threshold current for the transversal configuration is lower than that of the longitudinal configuration due to the factor $L_D / A_D^{1/2}$ affecting the radiation term in the inversion population (48b). From Fig. 10b, we

notice that although the threshold current increases with the transmission coefficient $\mathcal{T}$ according to (48), it remains under the maximum value of the injected current I_M that does not alter the normalization of the superradiant states.

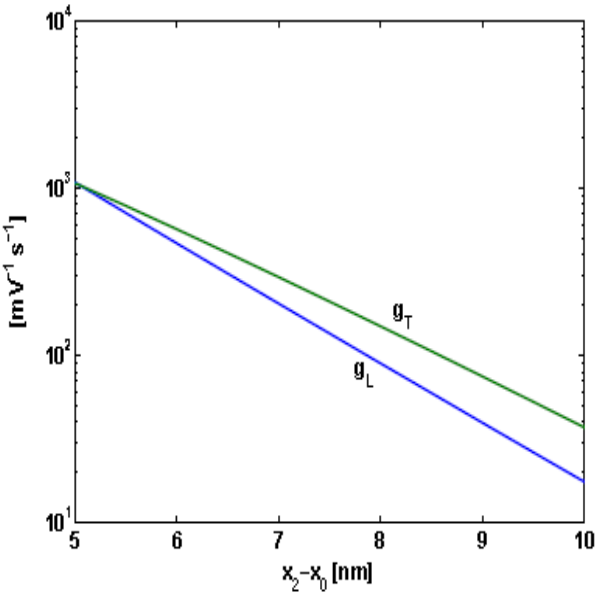

Fig. 9. The dependence of the coupling coefficients on the width of the i-zone.

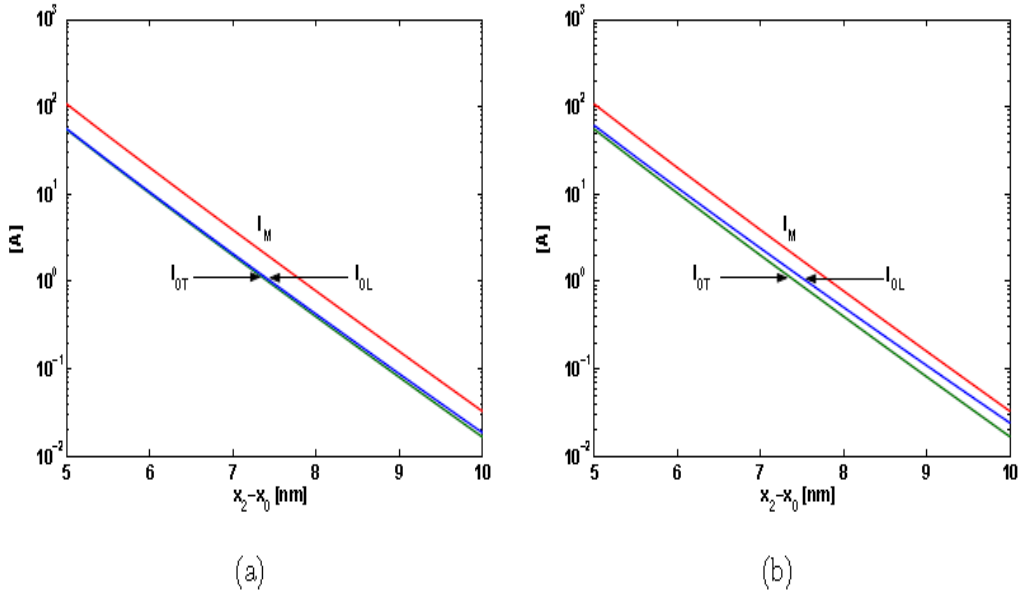

Fig. 10. The dependence of the threshold currents on the width of the i-zone for two values of the transmission coefficient of the output mirror: (a) $\mathcal{T} = 0.1$; (b) $\mathcal{T} = 0.5$.

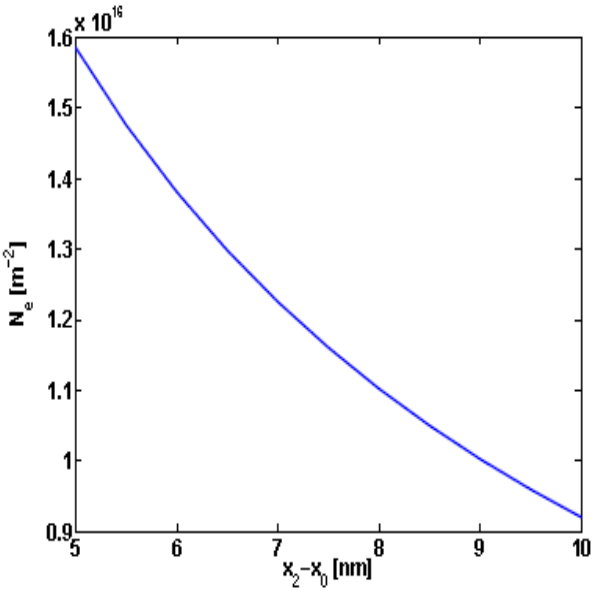

Fig. 11. The dependence of the quantum dot density on the width of the i-zone.

In Fig. 11 we represent the dependence on the width $x_2 - x_0$ of the quantum dot density N_e, obtained from the condition that the the entire internal field between the two regions n and p be contained between the two n_a and p_a arrays of the quantum dot system.

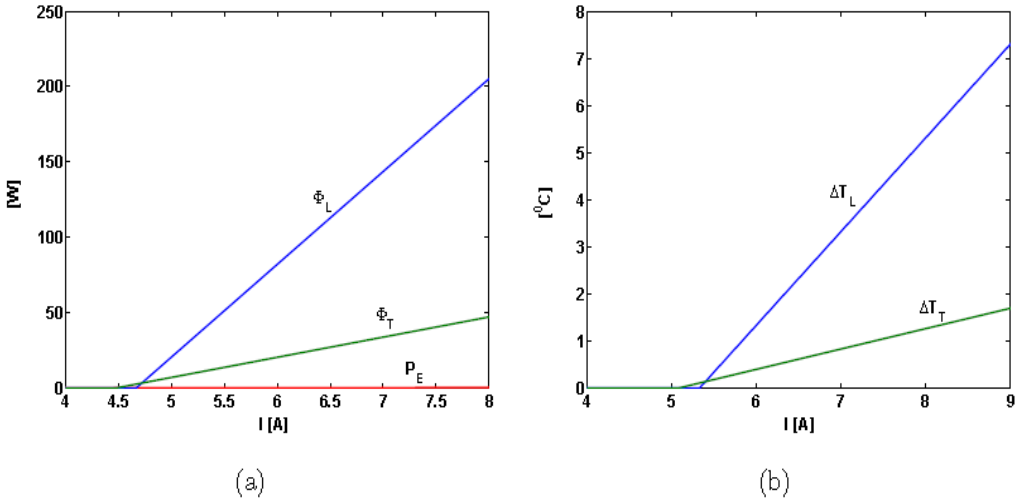

Fig. 12. (a) The radiation powers Φ_L and Φ_T and the electric power P_E as functions of the injection current I, for $x_2 - x_0 = 6.5nm$, $\mathcal{T} = 0.1$, and $\gamma_F = 10^7$ s−1;
(b) The temperature variations ΔT_L, ΔT_T as functions of the injection current I.

If this density is lower, spatial charge zones arise at the boundaries of the two conduction regions to complete the deficit of charge in the quantum dot region.

If this density is higher, a mobile charge is attracted at the boundaries of the conduction region to cancel the excess of charge in the quantum dot region. We notice that this dependence is rather weak.

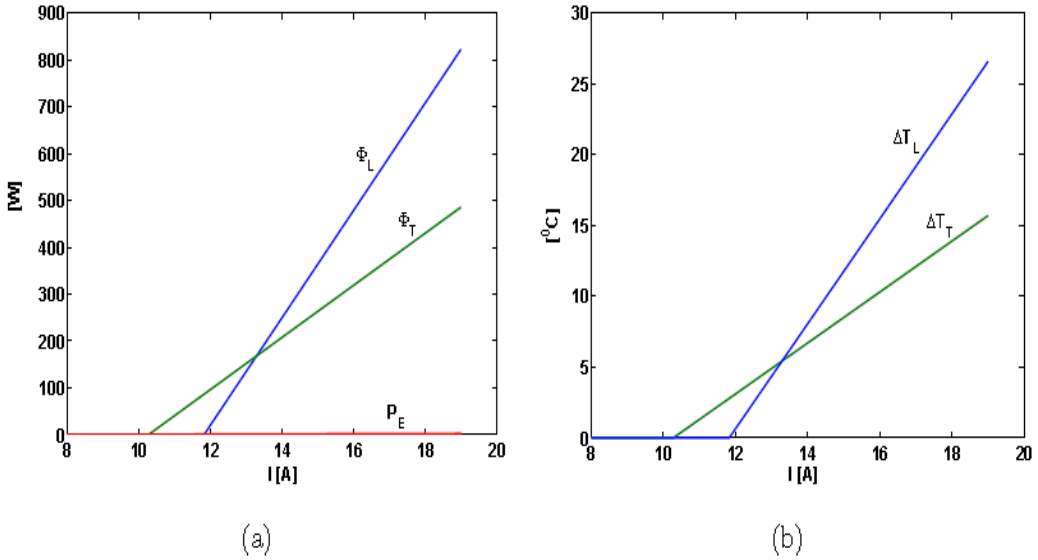

Fig. 13. The radiation powers Φ_L and Φ_T, the electric power P_E, and temperature variations ΔT_L, ΔT_T, as functions of the injection current I, for $x_2 - x_0 = 6.0\,nm$, $\mathcal{T} = 0.5$, and $\gamma_F = 10^7\ s^{-1}$.

In Fig. 12a we represent the radiation powers and the electric power for the longitudinal and transversal configurations, as functions of the current injected in the device. A radiation power arises only when the injection current exceeds a threshold value.

We notice that, due to the factor $L_D / A_D^{1/2}$ in the radiation term of the population inversion, the threshold current (48b) of a transversal device is lower than the threshold current (48a) of a longitudinal device.

However, due the same factor at the denominator of the radiation power (47b) of a transversal device, the increase with the injection current of this power is lower than that of the radiation power (47a) of a longitudinal one.

In Fig. 12b the total temperature variation in the semiconductor structure is represented.

We notice that a rather high power of $200\ W$, that means $0.5\ MW$ from an active area of $1\ m^2$, can be obtained at a rather low temperature difference of about $7\,°C$.

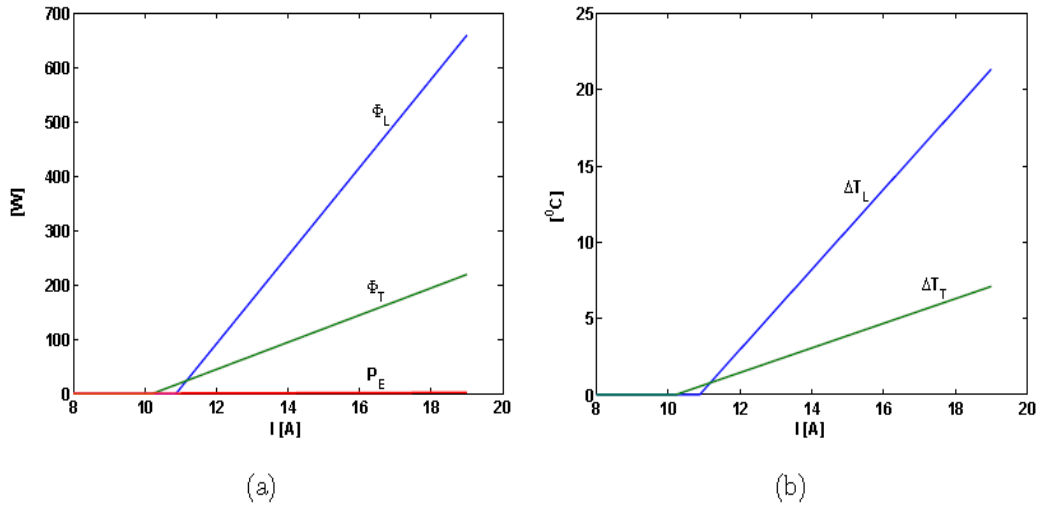

Fig. 14. The radiation powers Φ_L and Φ_T, the electric power P_E, and temperature variations ΔT_L, ΔT_T, as functions of the injection current I, for $x_2 - x_0 = 6.0nm$, $\mathcal{T} = 0.2$, and $\gamma_F = 10^7$ s^{-1}.

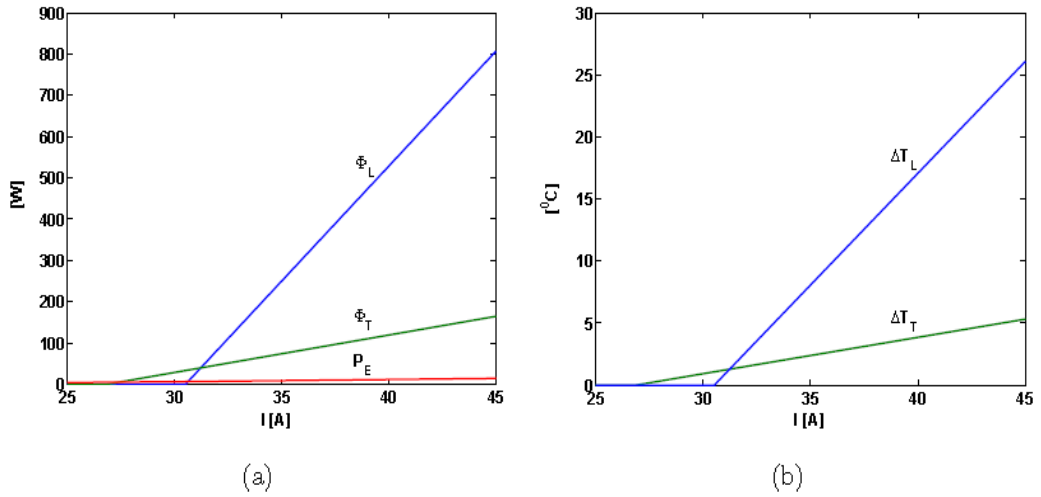

Fig. 15. The radiation powers Φ_L and Φ_T, the electric power P_E, and temperature variations ΔT_L, ΔT_T, as functions of the injection current, I for $x_2 - x_0 = 5.5nm$, $\mathcal{T} = 0.5$, and $\gamma_F = 10^8$ s^{-1}.

The radiation power of a transversal device becomes much higher increasing the transmission coefficient from $\mathcal{T} = 0.1$ to $\mathcal{T} = 0.5$ and also the transition dipole moment by diminishing the width of the i-zone from $x_2 - x_0 = 6.5nm$ to $x_2 - x_0 = 6.0nm$ as is represented in Fig. 13. In this case, the threshold current of the transversal device becomes significantly lower than that of the longitudinal

one. The threshold current of the longitudinal device can be lowered by decreasing the transmission coefficient as is represented in Fig. 14. It is remarkable that in the three cases represented in Figs. 12-14 the electric power dissipated by injecting a current in the device is much lower than the superradiant power. This is because, as one can notice also from (47), the superradiant power produced by the injected current corresponds to the high transition energy between the two zones n and p, while the power electrically dissipated by this current corresponds to a very low potential difference necessary for carrying this current through the two rather thin, highly conducting zones n and p. The difference between these two powers is obtained by heat absorption, when the electrons are excited from the potential of the p-zone to the higher potential of the n-zone of the next junction.

In Figs. 12-14, we considered a decay rate of the electromagnetic field $\gamma_F = 10^7\, s^{-1}$. The threshold currents (48a) and (48b) remain lower than the maximum current also for a larger decay rate of the electromagnetic field as $\gamma_F = 10^8\, s^{-1}$ (Fig. 15).

6. Non-Markovian fluctuations

Non-Markovian fluctuations are time-evolutions of polarization, population and field due to the self-consistent field of the environment particles that, in our case, are the quasifree electrons and holes in the conduction regions of the device. In Fig. 16, we represent the dynamics of a longitudinal device with a width of the i-zone $x_2 - x_0 = 5.5\, nm$ and a transmission coefficient of the output mirror $\mathcal{T} = 0.1$, while the threshold current is $I_{0L} = 24.1149\, A$ and the maximum current is $I_M = 46.0995\,\mathrm{A}$. We consider a step current of amplitude $I = 45\, A$ injected at time $t = 0$. In the Markovian approximation, a superradiant power $\Phi_L(t)$ is generated as in Fig. 16a, while the population $w(t)$ and polarization variables $u(t)$, $v(t)$ have the time-evolutions represented in Fig. 16b. At $t = 0$, the population increases from the equilibrium value w_T for the temperature T, to $w(0) = w_T + 2I/(eN_e A_D \gamma_\parallel)$ and, after that, while the radiation field increases, the population decreases tending to an asymptotic value. With an appropriate choice of the phase of the initial polarization, $v(0) = 0$, while $u(0)$ takes a value corresponding to the maximum value $-w_T$ of the Bloch vector, which is $u(0) = \sqrt{\left[w_T^2 - w^2(0)\right]/(2 - \mathcal{T})}$. In the Markovian approximation, the electromagnetic power is growing to a certain value, and after a short oscillation tends to the asymptotic value that according to (47a) is $P_L = 1.2843 \times 10^3 W$.

However, in the non-Markovian approximation, random fluctuations of the polarization, population, and field arise.

In Fig. 16, we consider such a fluctuation arising at a certain moment of time. In equations (21a) and 21b), we take a positive fluctuation with a duration $\tau_n = 1/\gamma_n = 2.6305 \times 10^{-12}\, s$, followed by a negative one with the same duration. From Fig. 16b, we notice that the polarization variables $u(t)$, $v(t)$ undergo very rapid variations, which start a much longer evolution of these variables and of the radiation field (Fig. 16a). In Fig. 16c, these rapid variations are represented in a short timescale.

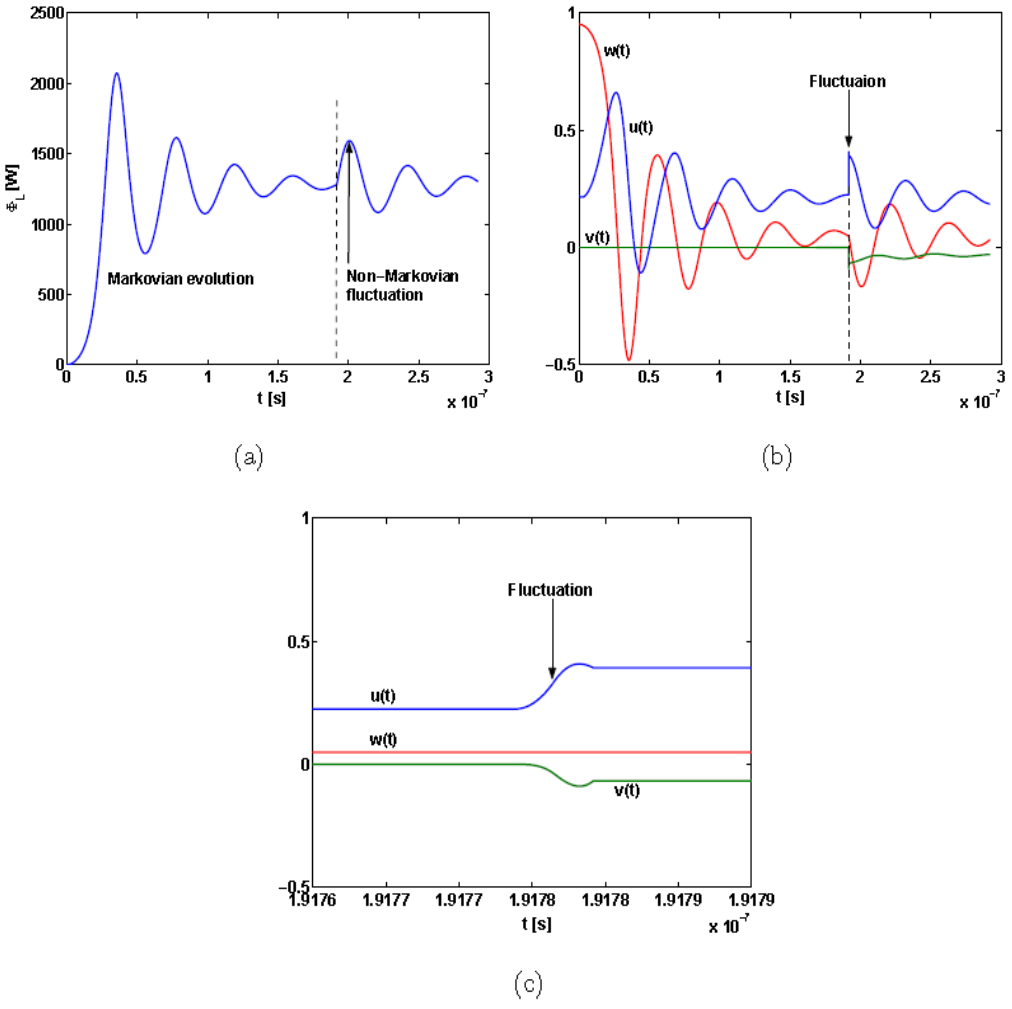

Fig. 16. Dynamics of a longitudinal superradiant device with $x_2 - x_0 = 5.5\, nm$ and $\mathcal{T} = 0.1$ when a step current of I = 45 A is injected in the device: a) superradiant power; b) polarization and population; c) polarization fluctuation in a short timescale.

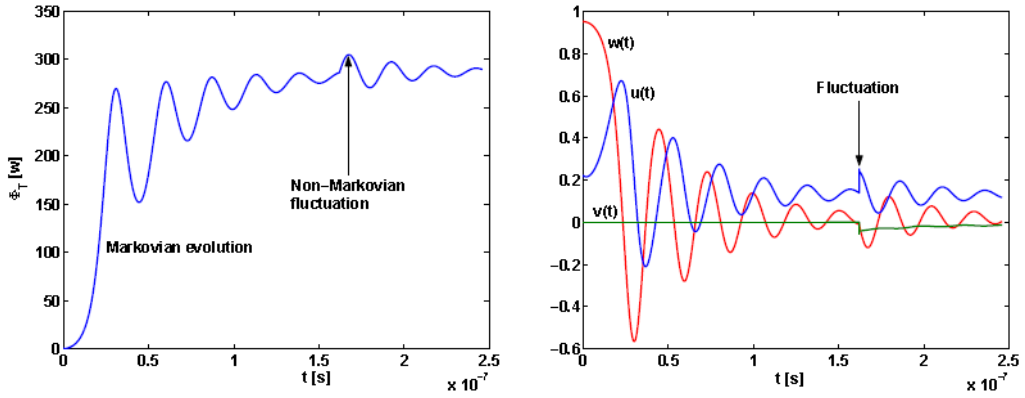

Fig. 17. Dynamics of a transversal superradiant device with $x_2 - x_0 = 5.5nm$ and $\mathcal{T} = 0.1$ when a step current of $I = 45\,A$ is injected.

In Fig. 17, we represent the dynamics of the transversal device with the same semiconductor structure and injected current, while the threshold current takes a lower value $I_{0T} = 23.4528\,A$. We notice that, while the radiation power is lower, this device is much less sensitive to the thermal fluctuations described by the non-Markovian term. In Figs. 16 and 17, we considered a positive fluctuation followed by a negative one, which means an integration over a first interval of time $\tau_n = 1/\gamma_n$ with a phase $\phi_n = 0$ followed by an integration over a second interval of time τ_n with a phase $\phi_n = \pi$. Changing the phases of the fluctuations, i.e. a negative fluctuation followed by a positive one (Figs. 18 and 19), we get similar evolutions but with opposite signs.

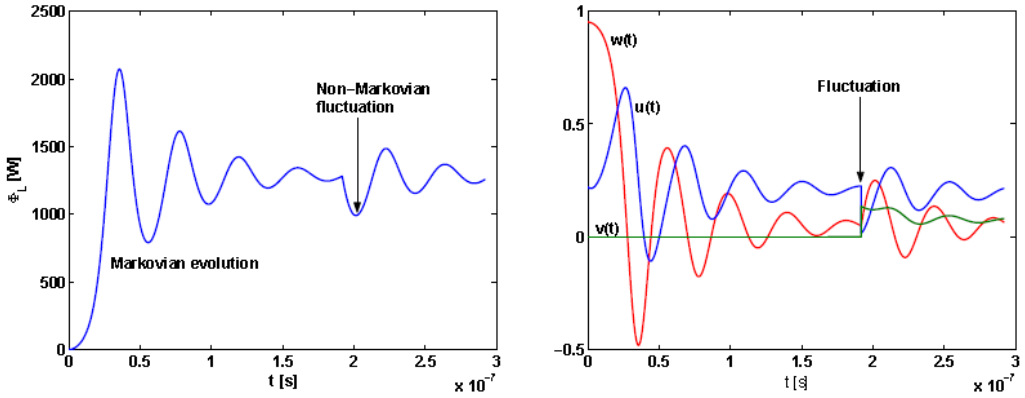

Fig. 18. Dynamics of a longitudinal superradiant device with a negative fluctuation $(\phi_n = \pi)$, followed by a positive one $(\phi_n = 0)$.

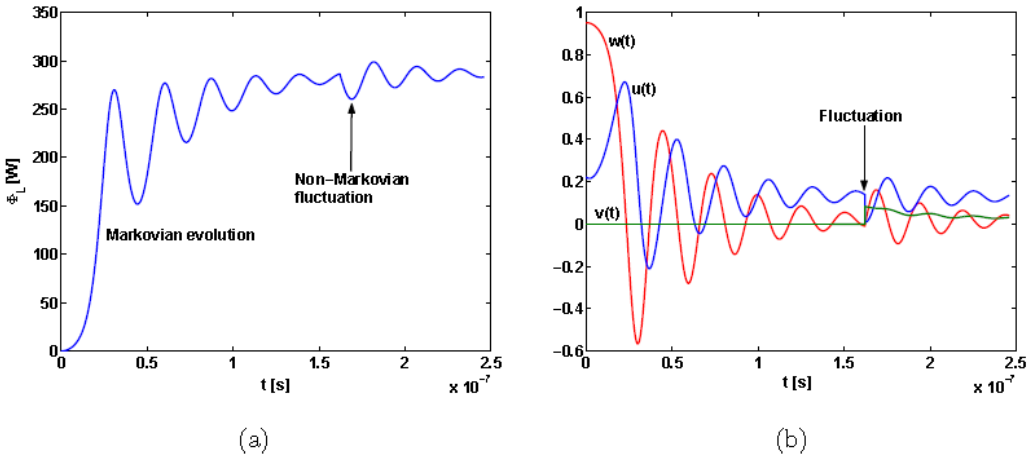

Fig. 19. Dynamics of a transversal superradiant device with a negative fluctuation $(\phi_n = \pi)$, followed by a positive one $(\phi_n = 0)$.

Conclusions

On the basis of a non-Markovian master equation for a system of Fermions interacting with a mode of the electromagnetic field, we derived polarization equations with additional terms for the thermal fluctuations of the environment particles, a population equation with an additional term for a current injected in the system, and field equations with additional terms for the radiation of the field. We performed numerical calculations for a realistic semiconductor device including a number of n-i-p superradiant junctions connected in series. A superradiant power that is significant for applications is obtained for quite feasible values of the physical parameters.

While a current is injected in the semiconductor structure, the most part of the transition energy is converted into coherent electromagnetic energy, a smaller part is transfered to the crystal vibrations, a still smaller part is dissipated in the conduction regions, and a quite negligible part is emitted as thermal radiation. The electron transfer through the quasi-ohmic contacts between the superradiant junctions is provided with energy by heat absorption from the environment.

The coupling of the superradiant electron system to the crystal vibrations mainly determines the threshold current of the device. This coupling is very sensitive to the transition energy, the corresponding decay rate being proportional to this energy with power 5, while the decay rate for the coupling to the conduction electrons gets smaller with the transition energy. These dependences can be understood in physical terms.

Thus, the decrease of the electric decay rate with the transition energy is an effect of the decrease of the dipole moment of the conduction electrons that, at higher energies in the conduction band, have states with more rapidly oscillating in space wave functions. This decrease of the dipole moment dominates the increase with the transition energy of the density of states in the decay rate. The increase of the phonon decay rate with the transition energy can be understood by the increase of the density of states and of the interaction potential with this energy. However, the density of these phonon states increases with the transition energy as long as their wavelength is much longer than the distance between atoms. When the phonon wavelength approaches the distance between atoms, the density of phonon states can no more be considered as quasi-continuous and, for energies that are not in resonance with the vibrational modes, the coupling begins to decrease, finally vanishing as in the Mösbauer effect. In our case of rather low transition energies, when the phonon states can be considered quasi-continuous, an optimum value of the transition energy exists, when the decay rate and, consequently, the threshold injection current take the minimum value. However, this minimum value of the the threshold current could not be very advantageous for a high superradiant power. A decrease of the threshold current means a decrease of the current injected in the device that cannot be much larger than the threshold value, otherwise altering the normalization of the active electron distribution in the two quantum states and, by this, dramatically altering the difference between the corresponding energy levels. A larger decay rate enables a larger injected current and, consequently, a larger superradiant power as long as the threshold current I0L (I0T) remains significantly lower than the maximum current IM.

We studied two versions of this superradiant device: (1) a longitudinal one, with the the superradiant field propagating in the same direction as the injected current, and (2) a transversal one, with the superradiant field propagating perpendicularly to the direction of the injected current, i.e. in the plane of the semiconductor structure. We derived analytical expressions of the superradiant power for the two devices in a stationary regime, and numerically solved the time-dependent equations of population, polarization, and field in the Markovian approximation. In these equations, the non-Markovian dynamics is described by a time-integral of the polarization variables multiplied with harmonic functions with a frequency equal to the fluctuation rate *n*, and a random phase with the fluctuation time $\tau_n = 1/\gamma_n$.

For the physical system considered here, the fluctuation time is much shorter than the decay time: $\tau_n << 1/\gamma_{\|}$. When such a fluctuation of the non-Markovian term arises at a certain moment of time, a long-standing evolution of the radiation power, population, and polarization is started. The amplitude of such a fluctuation of the superradiant power is far from being negligible, but consists only in an oscillation round the Markovian value.

R E F E R E N C E S

[1] Eliade Stefanescu and Lucian Ring-Cornescu, *Longitudinal Quantum Heat Converter*, U.S. Patent Office, Appln No. 11/773, 793 (July 5, 2007).

[2] Eliade Stefanescu and Lucian Ring-Cornescu, *Transversal Quantum Heat Converter*, U.S. Patent Office, Appln No. 11/773, 850 (July 5, 2007).

[3] Eliade Stefanescu and Lucian Ring-Cornescu, *Quantum Injection System*, U.S. Patent Office, Appln No. 11/773, 862 (July 5, 2007).

[4] E. Stefanescu, W. Scheid, Physica A 374 (2007) 203.

[5] E. Stefanescu, W. Scheid, and A. Sandulescu, Annals of Physics 323 (2008) 1168.

[6] E. Stefanescu, Physica A 350 (2005) 227.

[7] V. M. Axt, and S. Mukamel, Rev. Mod. Phys. 70 (1998) 145.